Position Sensorless Drive and Online Parameter Estimation for Surface-Mounted PMSMs Based on Adaptive Full-State Feedback Control

Yao, Yu; Huang, Yunkai; Peng, Fei; Dong, Jianning

DOI
10.1109/TPEL.2019.2957058

Publication date
2020

Document Version
Final published version

Published in
IEEE Transactions on Power Electronics

Position Sensorless Drive and Online Parameter Estimation for Surface-Mounted PMSMs Based on Adaptive Full-State Feedback Control

Yu Yao, *Student Member, IEEE*, Yunkai Huang, Fei Peng, *Member, IEEE*, and Jianning Dong, *Member, IEEE*

***Abstract*—In this article, a position sensorless drive and online parameter estimation method for surface-mounted permanent magnet synchronous machines-based on adaptive full-state feedback current control is proposed. The position sensorless drive is established by the detection of the back-electromotive force in the $\gamma\delta$ synchronous reference frame, which is effective at the medium-speed and high-speed range. Besides, accurate estimation of the winding resistance, the stator inductance, and the flux linkage of the PM is achieved independently. Compared with the traditional recursive-least-square methods, the proposed parameter identification method can be easily implemented because of the significantly reduced execution time. With the help of the parameter identification, the precise position estimation can be achieved by the proposed sensorless control method regardless of the parameter variation during the operation. The stability of the proposed method is proved by the Lyapunov-function method. Finally, the effectiveness of the proposed method is validated by the simulation and experimental results.**

***Index Terms*—Lyapunov function, parameter estimation, position sensorless drive, surface-mounted permanent magnet synchronous machines (PMSM).**

I. Introduction

With its advantages of high efficiency and high power density, permanent magnet synchronous machines (PMSMs) are widely used in applications including electric vehicles, industrial drives, household appliances, and so on. Among various control strategies for PMSMs, field-oriented control (FOC) is one of the mainstream methods. Normally, precise rotor position information is needed for FOC, and is usually obtained through the encoder or resolver mounted on the rotor shaft. However, the rotor position sensor not only inevitably increases the cost but also reduces system reliability. Therefore, the position sensorless control of PMSMs draws significant attention in both industry and academia.

The position estimation methods for PMSMs with continuous current waveform could be divided into two categories: Salient effect-based methods and back-electromotive force (EMF)-based methods. Generally, salient effect based methods [1]–[4] are applied when the operating velocity is relatively low. When the velocity is adequately high to obtain the back-EMF, the back-EMF-based observer is preferred because of the elimination of high frequency current injection. In this article, the wildly used surface mounted PMSM is studied, and the operating frequency is relatively high. Therefore, this article only focuses on the back-EMF-based methods.

Generally, the back-EMF-based methods rely on the estimation of back-EMF or the stator flux in the stationary $\alpha\beta$ reference frame or in the estimated rotational $\gamma\delta$ coordinate based on motor models. According to the designed structure, the estimation methods mainly include the sliding-mode methods [5]–[7], adaptive methods [8]–[11] and, the extended Kalman filter methods [12], etc. Moreover, these back-EMF-based methods can be classified into two classes: 1) Methods based on accurate parameters. 2) Methods considering parameter variation.

In [6], a novel sliding-mode rotor position observer with the sigmoid function to reduce chattering is proposed. An EMF observer is constructed to extract the back-EMF signal. Bernardes *et al.* [7] proposes a position estimation method with the discrete-time sliding-mode current observer. An adaptive EMF observer in order to improve the dynamic performance is also proposed. Piippo *et al.* [9] develops a speed-adaptive observer augmented with signal injection technique at low speed. In this way, the controller is able to operate stably at zero speed. And in [11], a position sensorless speed-control method based on an adaptive synchronous-frequency tracking-mode observer(ATFO) is proposed. It can estimate back-EMF accurately without being influenced by the harmonic components. In [10], an adaptive full-order observer is proposed to accomplish both stability and good dynamic response. Besides, the robustness against stator resistance and inductance variation is also investigated. But the experimental result demonstrates that when $|\Delta L|$ is over 20%, the estimated rotor position will be up to about 6 degree. However, the abovementioned methods are all based

Manuscript received July 14, 2019; revised October 14, 2019; accepted November 26, 2019. Date of publication November 28, 2019; date of current version March 13, 2020. This work was supported in part by National Natural Science Foundation of China under Grant 51777034 and Grant 51707037 and in part by the Natural Science Foundation of Jiangsu Province of China under Grant BK20161426. Recommended for publication by Associate Editor Prof. Dian Guo Xu. *(Corresponding author: Yunkai Huang.)*

Y. Yao, Y. Huang, and F. Peng are with the School of Electrical Engineering, Southeast University, Nanjing 210096, China (e-mail: yuyao@seu.edu.cn; huangyk@seu.edu.cn; pengfei@seu.edu.cn).

J. Dong is with the Delft University of Technology, Delft 2628 CD, The Netherlands (e-mail: j.dong-4@tudelft.nl).

This article has supplementary downloadable multimedia material available at http://ieeexplore.ieee.org provided by the authors.

Color versions of one or more of the figures in this article are available online at http://ieeexplore.ieee.org.

Digital Object Identifier 10.1109/TPEL.2019.2957058

on the accurate motor parameters. The accuracy of rotor position estimation depends on the accuracy of motor parameters directly.

The variation or inaccuracy of the machine parameters often occurs in the PMSM drive. The winding resistance and the PM flux linkage vary as the change of the temperature. Besides, the stator inductance cannot be accurately measured and is also variable resulting from the magnetic saturation. Inevitably, these undesirable parameter variations deteriorate the sensorless accuracy. So the online parameter identification for a sensorless PMSM drive system is necessary to achieve the precise position observation. In the PMSM parameter estimation, the winding resistance and the stator inductance are regarded as unknown parameters to be estimated. Besides, due to the necessary position sensorless drive, the back-EMFs are also unknown. Therefore, there are more than two unknown parameters in two equations of the PMSM model and the well-known rank-deficient problem exists. Moreover, the existing parameter estimation methods [13]–[19] based on a position sensored system cannot be effective for a sensorless drive system.

In order to solve this problem, some researchers have made significant contributions to achieve the online parameter estimation for a sensorless PMSM driving system. One effective method to solve the rank-deficient problem is that several parameters are estimated online while the remaining electrical parameters are treated as the nominal values. In [20], multiparameter estimation for the resistance and the flux linkage using the model reference adaptive system (MRAS) method is performed while the stator inductance is treated as a known parameter. So the estimation accuracy is sensitive to the foreknown inductance. In [21], an online parameter identification method and sensorless control using identified parameters are achieved in both surface-mounted PMSM and interior PMSM. A recursive least-square method which are not affected by the position estimation error is proposed to estimate the winding resistance and dq-axis inductance. But the experimental results demonstrate the ill-convergence performance of the resistance identification. Besides, the PM flux linkage is regarded as known and the variation of the flux linkage deteriorates the identification accuracy. Hamida *et al.* [22] proposes an adaptive interconnected observer with the rotor speed, the rotor position, the load torque, the stator inductance, and the resistance estimated at the same time. But the flux linkage is also treated as a known parameter. And the proposed observer is quite complicated with matrix manipulations. As the experimental results shown, the estimation error of the rotor position is up to 0.2 rad, which is relatively large.

Several papers investigate the parameter estimation method which does not need to assume one or two parameters as known parameters. Piippo *et al.* [23] proposes an online method for the estimation of the stator resistance and the PM flux linkage for Sensorless PMSM drives. The resistance will be estimated at low speed while the flux linkage is estimated at medium and high speed. But the influence of the inductance variation is also not considered. In [24], a supertwisting algorithm based on second-order sliding-mode observer (STA-SMO) with online stator resistance estimation for nonsalient PMSMs is proposed. The winding resistance can be estimated independently, but only the variation of the resistance is considered and actually, in high-speed region, the variation of the inductance is more important. In [25], a two time-scale affine projection approach is developed to accurately estimate the stator resistance and dq-axis inductance for a model-based sensorless control of interior PMSMs. But the proposed parameter estimation method needs to update the estimated extended EMF (EEMF) from the sensorless observer and meanwhile, the identified parameters are also adopted in the sensorless observer to estimate the EEMF. In that case, an inner loop between the parameter estimation and the EEMF observer is established, but the proof of the stability is not provided. Besides, the experimental results shows the position error can be reduced to 86%, which indicates the estimation error of these parameters is still large.

To overcome the rank-deficient and ill-convergence problem for a sensorless PMSM drive system, this article proposes a position sensorless drive and online parameter estimation method for surface-mounted PMSM (SPMSM) based on adaptive full-state feedback current control. The position sensorless drive relies on the detection of the back-EMF in the $\gamma\delta$ synchronous reference frame, which can be effective at the medium and high speed range. In order to estimate the parameters of the PMSM, a sinusoidal signal is injected into the γ axis. Accurate estimation of the winding resistance, the stator inductance and the back-EMF is achieved independently regardless of the position estimation error. With the estimated parameters updated, the precise estimation of the back-EMF can be achieved despite the parameter variation during the operation. From the estimated back-EMF, both the flux linkage of the PM and the position error can be calculated directly. Finally, a phase-locked loop (PLL) is implemented to observe the rotor position according to the calculated position error. The stability of the proposed method is given by the Lyapunov-function method. The selection method of the gains and the injected signal is also provided.

This article is organized as follows. Section II describes the electrical model of the SPMSM and the model in $\gamma\delta$ synchronous reference frame is used to design the proposed method. Section III presents the proposed method and the proof of the stability. In Section IV, the convergent performance of the estimated parameters and the estimated back-EMF is analyzed in details. Section V demonstrates the digital implementation and the selection of gains. Finally, the simulation and experimental results are provided in Section VI to validate the effectiveness of the proposed method. Section VII concludes this article.

II. Electrical Model of SPMSMs

In this section, the model of the SPMSM is developed in the stationary $\alpha\beta$ reference frame, the synchronous dq reference frame, and the estimated rotational $\gamma\delta$ synchronous reference frame, respectively.

Neglecting the cross-coupling magnetic saturation, iron loss, and the nonlinearity of the voltage source inverter (VSI), the

model of the SPMSM in the $\alpha\beta$ coordinate is derived as

$$u_\alpha = Ri_\alpha + L\dot{i}_\alpha + e_\alpha$$
$$u_\beta = Ri_\beta + L\dot{i}_\beta + e_\beta \quad (1)$$

where R is the winding resistance, L is the stator inductance, and i, u, e represent the stator current, stator voltage, and the back-EMF, respectively. Additionally, there is

$$e_\alpha = -\omega\psi_m \sin\theta$$
$$e_\beta = \omega\psi_m \cos\theta \quad (2)$$

where ω is the electrical angular speed, θ is the electrical rotor position, and ψ_m is the rotor flux linkage.

Transforming (1) and (2) into synchronous dq reference frame, there will be

$$u_d = Ri_d + L\dot{i}_d - \omega L i_q$$
$$u_q = Ri_q + L\dot{i}_q + \omega L i_d + \omega\psi_m. \quad (3)$$

Since θ is not available in the position sensorless control method, the model of the SPMSM is built in the estimated $\gamma\delta$ reference frame and the transformation matrix is

$$\mathbf{T}_{dq\to\gamma\delta} = \begin{bmatrix} \cos\tilde{\theta} & -\sin\tilde{\theta} \\ \sin\tilde{\theta} & \cos\tilde{\theta} \end{bmatrix} \quad (4)$$

where the position error $\tilde{\theta} = \theta - \hat{\theta}$ and $\hat{\theta}$ is the estimated rotor position. Based on the transformation matrix, the model of the SPMSM in the $\gamma\delta$ reference frame can be obtained as

$$u_\gamma = Ri_\gamma + L\dot{i}_\gamma - \omega L i_\delta + e_\gamma + L\dot{\tilde{\theta}} i_\delta$$
$$u_\delta = Ri_\delta + L\dot{i}_\delta + \omega L i_\gamma + e_\delta - L\dot{\tilde{\theta}} i_\gamma \quad (5)$$

with

$$e_\gamma = -\omega\psi_m \sin\tilde{\theta}$$
$$e_\delta = \omega\psi_m \cos\tilde{\theta}$$
$$\dot{e}_\gamma = -e_\delta\dot{\tilde{\theta}} - \omega\dot{\psi}_m \sin\tilde{\theta}$$
$$\dot{e}_\delta = e_\gamma\dot{\tilde{\theta}} + \omega\dot{\psi}_m \cos\tilde{\theta} \quad (6)$$

Normally, the dynamic response of the $\dot{\tilde{\theta}}$ is relatively slower compared with the electrical process. Therefore, the $L\dot{\tilde{\theta}} i_\delta$ and $L\dot{\tilde{\theta}} i_\gamma$ are neglected in this article. Finally, the developed model of the SPMSM in $\gamma\delta$ reference frame is simplified as follows:

$$u_\gamma = Ri_\gamma + L\dot{i}_\gamma - \omega L i_\delta + e_\gamma$$
$$u_\delta = Ri_\delta + L\dot{i}_\delta + \omega L i_\gamma + e_\delta. \quad (7)$$

III. Proposed Method

In this section, a position sensorless drive and online parameter estimation method for SPMSM based on adaptive full-state feedback current control is proposed. The proposed method can accurately estimate the winding resistance, the inductance, and the back-EMF in $\gamma\delta$ synchronous frame. The stability of the proposed method can be proved by the Lyapunov-function method.

A. Adaptive Full-State Feedback Current Control

Based on (7) and (6), the proposed adaptive current controller is designed in the $\gamma\delta$ coordinate as

$$u_{\gamma c} = \hat{R}i_{\gamma\_\mathrm{ref}} + \hat{L}\dot{i}_{\gamma\_\mathrm{ref}} - \omega\hat{L}i_\delta + \hat{e}_\gamma + k_{ei}e_{i\gamma}$$
$$u_{\delta c} = \hat{R}i_{\delta\_\mathrm{ref}} + \hat{L}\dot{i}_{\delta\_\mathrm{ref}} + \omega\hat{L}i_\gamma + \hat{e}_\delta + k_{ei}e_{i\delta} \quad (8)$$

where

$$e_{i\gamma} = i_{\gamma\_\mathrm{ref}} - i_\gamma$$
$$e_{i\delta} = i_{\delta\_\mathrm{ref}} - i_\delta \quad (9)$$

where k_{ei} is a positive gain and the superscript $\hat{}$ refers to the estimated values.

1) Exact Parameter Adopted: When the estimated values ($\hat{R}$, $\hat{L}$, $\hat{e}_\gamma$, and $\hat{e}_\delta$) are equivalent to their real values, the dynamic response of closed-loop system with the proposed control method can be derived as

$$Ri_\gamma + L\dot{i}_\gamma = Ri_{\gamma\_\mathrm{ref}} + L\dot{i}_{\gamma\_\mathrm{ref}} + k_{ei}e_{i\gamma}$$
$$Ri_\delta + L\dot{i}_\delta = Ri_{\delta\_\mathrm{ref}} + L\dot{i}_{\delta\_\mathrm{ref}} + k_{ei}e_{i\delta} \quad (10)$$

and

$$\dot{e}_{i\gamma} = -\frac{k_{ei}+R}{L}e_{i\gamma}(t)$$
$$\dot{e}_{i\delta} = -\frac{k_{ei}+R}{L}e_{i\delta}(t). \quad (11)$$

Therefore, $e_{i\gamma}$ and $e_{i\delta}$ will exponentially asymptotically converge to zero and the rate of the convergence depends on the selection of k_{ei}.

2) Adaptive Parameter Adopted: When the adaptive parameters adopted in the controller, the dynamic response of the closed-loop system with the proposed method can be derived as

$$L\dot{e}_{i\gamma} = (R-\hat{R})i_{\gamma\_\mathrm{ref}} - Re_{i\gamma} + (L-\hat{L})\dot{i}_{\gamma\_\mathrm{ref}} - \omega\tilde{L}i_\delta + e_\gamma - \hat{e}_\gamma - ke_{i\gamma}$$
$$L\dot{e}_{i\delta} = (R-\hat{R})i_{\delta\_\mathrm{ref}} - Re_{i\delta} + (L-\hat{L})\dot{i}_{\delta\_\mathrm{ref}} + \omega\tilde{L}i_\gamma + e_\delta - \hat{e}_\delta - ke_{i\delta}. \quad (12)$$

For simplified marking, there is

$$\frac{d}{dt}e_{i\gamma} = -\frac{k_{ei}+R}{L}e_{i\gamma} + \frac{\tilde{R}}{L}i_{\gamma\_\mathrm{ref}} + \frac{\tilde{L}}{L}\dot{i}_{\gamma\_\mathrm{ref}} - \omega\frac{\tilde{L}}{L}i_\delta + \frac{1}{L}\tilde{e}_\gamma$$
$$\frac{d}{dt}e_{i\delta} = -\frac{k_{ei}+R}{L}e_{i\delta} + \frac{\tilde{R}}{L}i_{\delta\_\mathrm{ref}} + \frac{\tilde{L}}{L}\dot{i}_{\delta\_\mathrm{ref}} + \omega\frac{\tilde{L}}{L}i_\gamma + \frac{1}{L}\tilde{e}_\delta \quad (13)$$

where

$$\tilde{R} = R - \hat{R} \quad \tilde{L} = L - \hat{L}$$
$$\tilde{e}_\gamma = e_\gamma - \hat{e}_\gamma \quad \tilde{e}_\delta = e_\delta - \hat{e}_\delta \quad (14)$$

where $\tilde{R}$, $\tilde{L}$, $\tilde{e}_\gamma$, and $\tilde{e}_\delta$ are the estimation errors of R, L, e_γ, and e_δ. The closed-loop system is also stable, but the final value of $e_{i\gamma}$ and $e_{i\delta}$ with $\dot{i}_{\gamma\_\mathrm{ref}}$ and $\dot{i}_{\delta\_\mathrm{ref}}$ treated as zero at the steady state can be written as

$$|e_\gamma|_{\to\infty} = \left| \frac{\tilde{R} i_{\gamma\_\mathrm{ref}} - \omega \tilde{L} i_\delta + \tilde{e}_\gamma}{k_{ei} + R} \right|$$
$$|e_\delta|_{\to\infty} = \left| \frac{\tilde{R} i_{\delta\_\mathrm{ref}} + \omega \tilde{L} i_\gamma + \tilde{e}_\delta}{k_{ei} + R} \right|. \tag{15}$$

Clearly, the static tracking error occurs resulting from the mismatched parameters. Besides, this tracking error can be decreased by selecting a large k_{ei}, but the closed-loop system with a large k_{ei} will be more sensitive to the sampling noises. Therefore, it is significantly necessary to achieve the online parameters estimation and the small k_{ei} can be selected with good dynamic response and eliminated static tracking error.

B. Parameter Estimation Mechanism

A Lyapunov function is selected as

$$V = \frac{1}{2}{e_{i\gamma}}^2 + \frac{1}{2}{e_{i\delta}}^2 + \frac{1}{2Lk_R}\tilde{R}^2 + \frac{1}{2Lk_L}\tilde{L}^2 + \frac{1}{2Lk_e}\tilde{e}_\gamma^2 + \frac{1}{2Lk_e}\tilde{e}_\delta^2 \tag{16}$$

and then based on (13), the derivative of the selected Lyapunov function can be obtained as

$$\dot{V} = -\frac{k_{ei}+R}{L}({e_{i\gamma}}^2 + {e_{i\delta}}^2) + \frac{\tilde{R}}{L}W_R + \frac{\tilde{L}}{L}W_L + \frac{1}{L}\tilde{e}_\gamma e_{i\gamma} + \frac{1}{L}\tilde{e}_\delta e_{i\delta} + \frac{1}{Lk_R}\tilde{R}\dot{\tilde{R}} + \frac{1}{Lk_L}\tilde{L}\dot{\tilde{L}} + \frac{1}{Lk_e}\tilde{e}_\gamma\dot{\tilde{e}}_\gamma + \frac{1}{Lk_e}\tilde{e}_\delta\dot{\tilde{e}}_\delta. \tag{17}$$

To guarantee the seminegative definite of the derivative of the selected Lyapunov function, the estimation mechanism is chosen as follows.

1) Resistance and Inductance Estimation: In the drive of SPMSM, the winding resistance R varies with the temperature while the stator inductance L varies with the magnetic saturation. But the variation boundary of these two parameters and their maximum changing rate always exist. Therefore, it can be represented as

$$|\tilde{R}| \le \xi_R \quad |\dot{R}| \le \xi_{\dot{R}}$$
$$[1mm]|\tilde{L}| \le \xi_L \quad |\dot{L}| \le \xi_{\dot{L}} \tag{18}$$

where ξ_R and ξ_L denote the variation boundary of R and L. $\xi_{\dot{R}}$ and $\xi_{\dot{L}}$ are the maximum changing rate of the R and L.

Based on (18), the estimation mechanism of R and L is proposed as

$$\dot{\hat{R}} = \begin{cases} k_R W_R, & \hat{R} \in [\overline{R} - \xi_R \ \ \overline{R} + \xi_R] \\ k_R W_R, & \hat{R} \le (\overline{R} - \xi_R) \text{ and } W_R \ge 0 \\ k_R W_R, & \hat{R} \ge (\overline{R} + \xi_R) \text{ and } W_R \le 0 \\ 0, & \text{else} \end{cases}$$
$$\dot{\hat{L}} = \begin{cases} k_L W_L, & \hat{L} \in [\overline{L} - \xi_L \ \ \overline{L} + \xi_L] \\ k_L W_L, & \hat{L} \le (\overline{L} - \xi_L) \text{ and } W_L \ge 0 \\ k_L W_L, & \hat{L} \ge (\overline{L} + \xi_L) \text{ and } W_L \le 0 \\ 0, & \text{else} \end{cases} \tag{19}$$

with

$$W_R = i_{\gamma\_\mathrm{ref}} e_{i\gamma} + i_{\delta\_\mathrm{ref}} e_{i\delta}$$
$$W_L = \dot{i}_{\gamma\_\mathrm{ref}} e_{i\gamma} + \omega i_\gamma e_{i\delta} + \dot{i}_{\delta\_\mathrm{ref}} e_{i\delta} - \omega i_\delta e_{i\gamma} \tag{20}$$

where k_R and k_L are positive gains.

2) EMF and Flux Linkage Estimation: In order to achieve the position sensorless drive, the back-EMF is also necessary to be estimated. Normally, the back-EMF can be easily detected by a model-based observer, but in this article, a simplified estimation mechanism is proposed as

$$\dot{\hat{e}}_\gamma = -\hat{e}_\delta\dot{\hat{\theta}} + k_e e_{i\gamma}$$
$$\dot{\hat{e}}_\delta = \hat{e}_\gamma\dot{\hat{\theta}} + k_e e_{i\delta} \tag{21}$$

where k_e is a positive gain. The estimated position error can be obtained as

$$e_\theta(k) = \arctan\left(-\frac{\hat{e}_\gamma(k)}{\hat{e}_\delta(k)}\right) \tag{22}$$

where $e_\theta(k)$ is the estimated position error. A PLL can be implemented to observe the rotor speed and position from the $e_\theta(k)$. The more details of the PLL can be found in Section V. Additionally, the estimation of ψ_m can be obtained from the estimated back-EMF $\hat{e}_\gamma$ and $\hat{e}_\delta$ as

$$\hat{\psi}_m = \frac{\sqrt{\hat{e}_\gamma^2 + \hat{e}_\delta^2}}{\omega} \tag{23}$$

where the $\hat{\psi}_m$ is the estimated flux linkage of the PM.

C. Proof of Stability

The stability of the closed-loop system with the full-state current controller (8), the resistance and inductance estimator (19) and the back-EMF observer (21) driven will be proved by the Lyapunov-function method.

Substituting (19) and (21) into (17), it can be derived as

$$\dot{V} = -\frac{k_{ei}+R}{L}({e_{i\gamma}}^2 + {e_{i\delta}}^2) + \frac{1}{Lk_R}\tilde{R}\dot{R} + \frac{1}{Lk_L}\tilde{L}\dot{L} + \frac{\omega}{Lk_e}\dot{\psi}_m(-\tilde{e}_\gamma\sin\tilde{\theta} + \tilde{e}_\delta\cos\tilde{\theta}). \tag{24}$$

1) Constant Parameters: When the resistance R, the inductance L, and the PM flux linkage ψ_m are regarded as constant, there is a representation as

$$\begin{aligned}\dot{R} &\approx 0\\ \dot{L} &\approx 0\\ \dot{\psi}_m &\approx 0.\end{aligned} \tag{25}$$

When the predefined boundaries are appropriately selected, the estimator of R and L shown in (19) can be simplified as

$$\begin{aligned}\dot{\hat{R}} &= k_R W_R\\ \dot{\hat{L}} &= k_L W_L\end{aligned} \tag{26}$$

and therefore, it can be derived as

$$\begin{aligned}\dot{\tilde{R}} &= \dot{R} - \dot{\hat{R}} = -k_R W_R\\ \dot{\tilde{L}} &= \dot{L} - \dot{\hat{L}} = -k_L W_L.\end{aligned} \tag{27}$$

According to (24) and (27), the derivative of the selected Lyapunov function can be expressed as

$$\dot{V} = -\frac{k_{ei}+R}{L}\left({e_{i\gamma}}^2 + {e_{i\delta}}^2\right). \tag{28}$$

Therefore, $\dot{V}$ is seminegative definite, which indicates that $e_{i\gamma}$ and $e_{i\delta}$ will converge to 0. It is clear that L and R are positive, therefore,the convergence rate depends on the choice of the parameter k_{ei}.

2) Variable Parameters: For the estimation of the back-EMF and the variation rate of the flux linkage, there is

$$\begin{aligned}|\tilde{e}_\gamma| \le \xi_{e_\gamma} \quad |\tilde{e}_\delta| \le \xi_{e_\delta}\\ |\dot{\psi}_m| \le \xi_{\dot{\psi}_m}\end{aligned} \tag{29}$$

where ξ_{e_γ} and ξ_{e_δ} are the variation boundary of e_γ and e_δ. $\xi_{\dot{\psi}_m}$ denotes the maximum variation rate of ψ_m.

According to (16), it can be derived as

$$e_{i\gamma}^2 + e_{i\delta}^2 = 2\,V - \frac{\tilde{R}^2}{Lk_R} - \frac{\tilde{L}^2}{Lk_L} - \frac{\tilde{e}_\gamma^2}{Lk_e} - \frac{\tilde{e}_\delta^2}{Lk_e} \tag{30}$$

and the derivative of the selected Lyapunov function can be obtained as

$$\dot{V} = -\frac{k_{ei}+R}{L}(2V - P) + Q \tag{31}$$

with

$$\begin{aligned}P &= \frac{\tilde{R}^2}{Lk_R} + \frac{\tilde{L}^2}{Lk_L} + \frac{\tilde{e}_\gamma^2}{Lk_e} + \frac{\tilde{e}_\delta^2}{Lk_e}\\ &\le \frac{\xi_R^2}{Lk_R} + \frac{\xi_L^2}{Lk_L} + \frac{{\xi_{e\gamma}}^2}{Lk_e} + \frac{{\xi_{e_\delta}}^2}{Lk_e}\\ Q &= \frac{\tilde{R}\dot{R}}{Lk_R} + \frac{\tilde{L}\dot{L}}{Lk_L} + \frac{\omega}{Lk_e}\dot{\psi}_m(-\tilde{e}_\gamma \sin\tilde{\theta} + \tilde{e}_\delta \cos\tilde{\theta})\\ &\le \frac{\tilde{R}\xi_{\dot{R}}}{Lk_R} + \frac{\tilde{L}\xi_{\dot{L}}}{Lk_L} + \frac{\omega}{Lk_e}\xi_{\dot{\psi}_m}(\xi_{e_\gamma} + \xi_{e_\delta}).\end{aligned} \tag{32}$$

Clearly, both P and Q are bounded. Especially, when V satisfies

$$V \ge \frac{L}{2(k_{ei}+R)}Q + \frac{P}{2} \tag{33}$$

the derivative of V becomes negative and the tracking error of i_γ and i_δ will decrease. Therefore, the boundary of the tracking error can be derived as

$$\begin{aligned}&\sqrt{e_{i\gamma}^2 + e_{i\delta}^2}\\ &\le \sqrt{\frac{1}{k_{ei}+R}\left|\frac{\tilde{R}\dot{R}}{k_R} + \frac{\tilde{L}\dot{L}}{k_L} + \frac{\omega}{k_e}\dot{\psi}_m(-\tilde{e}_\gamma\sin\tilde{\theta} + \tilde{e}_\delta\cos\tilde{\theta})\right|}\\ &\le \sqrt{\frac{1}{k_{ei}+R}\left(\frac{\xi_R\xi_{\dot{R}}}{k_R} + \frac{\xi_L\xi_{\dot{L}}}{k_L} + \frac{\omega}{k_e}\xi_{\dot{\psi}_m}(\xi_{e_\gamma} + \xi_{e_\delta})\right)}.\end{aligned} \tag{34}$$

On basis of the equation above, considering the predefined boundary (ξ_R, ξ_L) and the maximum variation rates ($\xi_{\dot{R}}$, $\xi_{\dot{L}}$ and $\xi_{\dot{\psi}_m}$), the current tracking error can be decreased by the selection of k_R, k_L, k_e, and k_{ei}. In fact, the R is closely related to the operating temperature, which varies slowly. The change performance of ψ_m is the same as the resistance. For the variation of L, it will be changed suddenly due to the magnetic saturation caused by the current, but once the current is on the steady state, the variation of the L will be small. Therefore, the static current tracking error can be greatly reduced by the appropriate selection of k_R, k_L, k_e, and k_{ei}.

IV. Parameters Convergence

The adaptive control method suffers from parameter drifting resulting from the dissatisfaction of the persistent excitation of the reference signals [26]. In this section, the parameter convergent performance of the proposed adaptive control method is analyzed in detail. Additionally, to guarantee the convergence of the estimated parameters and eliminate the parameter drifting, an extra signal will be injected into γ axis to improve the parameters convergence.

A. Persistent Excitation

In the proposed adaptive method, as demonstrated in (28), when both $e_{i\gamma}$ and $e_{i\delta}$ converge to zero, the $\dot{V}$ will stay zero. In that case, the V will stop decreasing and may be nonzero. It indicates that the globally asymptotic convergence of the $e_{i\gamma}$ and $e_{i\delta}$ will be guaranteed by the selected Lyapunov-function method, but $\tilde{R}$, $\tilde{L}$, $\tilde{e}_\gamma$, and $\tilde{e}_\delta$ may not converge to zero. The same statement can be also applied in the case with the variable parameters.

After $e_{i\gamma}$ and $e_{i\delta}$ converge to 0, the error dynamic (13) can be rewritten as

$$\begin{aligned}0 &= \tilde{L}\dot{i}_{\gamma\_\mathrm{ref}} + \tilde{R}i_{\gamma\_\mathrm{ref}} - \omega\tilde{L}i_\delta + \tilde{e}_\gamma\\ 0 &= \tilde{L}\dot{i}_{\delta\_\mathrm{ref}} + \tilde{R}i_{\delta\_\mathrm{ref}} + \omega\tilde{L}i_\gamma + \tilde{e}_\delta.\end{aligned} \tag{35}$$

According to [26], when the reference signal satisfies the persistent excitation, the $\tilde{R}$, $\tilde{L}$, $\tilde{e}_\gamma$, and $\tilde{e}_\delta$ will converge to zero. However, if the persistent excitation is not satisfied, the parameter drifting possibly happens because of the existence of nonparametric uncertainties including measurement noise and disturbance. In that case, some of the estimated parameters will drift away from their desired values to some unreasonable

values. And the system driven by the proposed adaptive method will be unstable.

The condition of the persistent excitation can be expressed as follows [26]. There exists positive constants a and ζ such that for any time $t \geq 0$

$$\int_{t}^{t+\zeta} \mathbf{v}(\tau)\mathbf{v}^{T}(\tau)d\tau \geq a\mathbf{I} \tag{36}$$

with

$$\mathbf{v} = \begin{bmatrix} \dot{i}_{\gamma\_\mathrm{ref}} - \omega i_{\delta} & i_{\gamma\_\mathrm{ref}} & 1 & 0 \\ \dot{i}_{\delta\_\mathrm{ref}} + \omega i_{\gamma} & i_{\delta\_\mathrm{ref}} & 0 & 1 \end{bmatrix}^{T}. \tag{37}$$

The persistent excitation of $\mathbf{v}(t)$ implies that the vectors $\mathbf{v}(t)$ corresponding to different times t cannot always be linearly dependent. Clearly, when both i_{γ_ref} and i_{δ_ref} are direct component, which is the worst case, the persistent excitation is not satisfied.

B. Sinusoidal Signal Injection

Dead-zone is a common solution to the parameter drifting. When the tracking error is inside the selected dead-zone, the adaptation mechanism will be shut down to avoid the parameter drifting [26]. However, the estimation error is sensitive to the selection of the dead-zone. Besides, it is difficult to analyze the boundary of the estimation errors. Therefore, the dead-zone method is not suitable for this case.

To solve the dissatisfaction of the persistent excitation, in this article, the signal injection method is implemented to improve the richness of the reference signals. The selected signal is usually a sinusoidal wave and is injected into the γ axis in order not to affect the torque production of the PMSM. In this way, the i_{γ_ref} contains one sinusoidal component and the vector $\mathbf{v}(t)$ will always be linearly independent. The persistent excitation of $\mathbf{v}(t)$ is satisfied and all the estimated parameters can converge to zero.

V. Digital Implementation

In this section, digital implementation of the proposed adaptive method using Euler discretization is presented. Then the selection of the injected signal and the operating procedure of the proposed method are provided.

A. Discretization of the Proposed Method

In the full-digital implementation, the proposed adaptive control method can be discretized using the forward-Euler method. The system diagram with the proposed adaptive control is shown in Fig. 1.

The derivative of the reference current can be obtained by the forward-Euler method as

$$\begin{aligned} \dot{i}_{\gamma\_\mathrm{ref}} &\approx \frac{\Delta i_{\gamma\_\mathrm{ref}}(k)}{T} = \frac{i_{\gamma\_\mathrm{ref}}(k) - i_{\gamma\_\mathrm{ref}}(k-1)}{T} \\ \dot{i}_{\delta\_\mathrm{ref}} &\approx \frac{\Delta i_{\delta\_\mathrm{ref}}(k)}{T} = \frac{i_{\delta\_\mathrm{ref}}(k) - i_{\delta\_\mathrm{ref}}(k-1)}{T} \end{aligned} \tag{38}$$

with T being the sampling period.

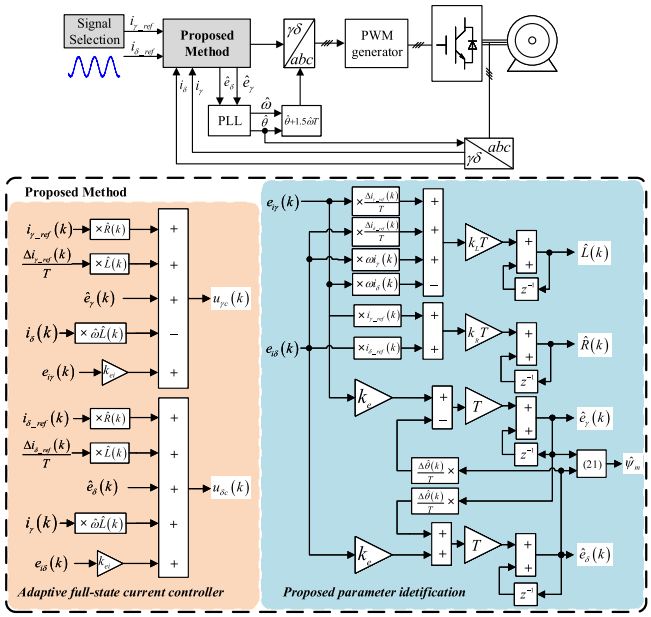

Fig. 1. System diagram with the proposed adaptive algorithm.

The $\frac{\Delta\hat{\theta}(k)}{T}$ is the discrete-time form of the $\dot{\hat{\theta}}$, which can be obtained from the discrete-time PLL. A classical discrete-time PLL can be designed as

$$\begin{aligned} \hat{\theta}(k+1) &= \hat{\theta}(k) + k_{\theta}e_{\theta}(k) + \hat{\omega}(k)T \\ \hat{\omega}(k+1) &= \hat{\omega}(k) + k_{\omega}e_{\theta}(k) \end{aligned} \tag{39}$$

where the k_{θ} and k_{ω} are positive parameters and the selection method can be found in [27]. The $\dot{\tilde{\theta}}$ can be also discretized by forward-Euler method as

$$\begin{aligned} \dot{\tilde{\theta}} &\approx \frac{\tilde{\theta}(k+1) - \tilde{\theta}(k)}{T} \\ &= \frac{\theta(k+1) - \hat{\theta}(k+1) - (\theta(k) - \hat{\theta}(k))}{T}. \end{aligned} \tag{40}$$

Considering $\theta(k+1) = \theta(k) + \omega(k)T$, based on (39), there is

$$\dot{\tilde{\theta}} \approx \frac{\omega(k)T - \hat{\theta}(k+1) + \hat{\theta}(k)}{T} = \frac{-k_{\theta}e_{\theta}(k)}{T} \tag{41}$$

and therefore $\Delta\hat{\theta}(k) = -k_{\theta}e_{\theta}(k)$.

B. Gains and Injected Signal Selection

For the selection of k_{ei}, based on (13), it can be derived as

$$0 \leq 1 - \frac{T}{L}(k_{ei} + R) < 1 \tag{42}$$

and

$$-R < k_{ei} \leq \frac{L}{T} - R. \tag{43}$$

The larger the k_{ei} is chosen, the faster the system converges. But in fact, the large feedback gain k_{ei} will bring more sampling noising to the system and will weaken the robustness of the control system. Therefore, the choice of the parameter k_{ei} will be

a tradeoff between the dynamic performance and the robustness requirements.

The selection of the gains and the injected signal is based on the following consideration:

1) According to (34), the large gains can decrease the current tracking error.
2) According to (19) and (21), the large gains can increase the convergent rate of the estimated parameters, but because of the inevitable current ripple caused by the pulse width modulation (PWM) and sampling noise, the large gains will cause the undesirable and unacceptable fluctuation of the estimated parameters. Especially, the fluctuation is also related to the amplitude and frequency of the injected signal.
3) For the high-speed region, the voltage margin is limited to the selection of the injected signals. So the selected signal has to be as small as possible.

Based on these considerations, these gains can be decided as follows.

1) Selection of k_R: Based on (34), in order to reduce the tracking error caused by the variation of R, k_R can be selected as

$$k_R \geq 10\xi_R\xi_{\dot{R}}. \tag{44}$$

Additionally, the discretized form of the resistance estimation can be obtained in Fig. 1 and the increment per sampling period of the $\hat{R}$ can be derived as

$$|\Delta\hat{R}(k)| = k_R T|i_{\gamma\_\mathrm{ref}}(k)e_{i\gamma}(k) + i_{\delta\_\mathrm{ref}}(k)e_{i\delta}(k)| \tag{45}$$

1) To obtain the fast convergent rate, the $|\Delta\hat{R}(k)|$ has to be adequately large. For the i_{δ_ref}, it is a direct component and the $e_{i\delta}(k)$ is so small that can be neglected on the steady state. The i_{γ_ref} and $e_{i\gamma}(k)$ contains the injected sinusoidal component, so the multiply of these two items consists of a direct component and a double-injected-frequency component. Because of the integrator in the estimation of R, the high frequency component is well filtered. And the direct component depends on the phase difference between $i_{\gamma\_\mathrm{ref}}(k)$ and $e_{i\gamma}(k)$. In this article, the phase difference is selected to be 0.25π and more details can be found in Appendix. So there is

$$k_R \geq \frac{2.83|\Delta\hat{R}(k)|_{\min}}{T|i_{\gamma\_\mathrm{ref}}(k)||e^f_{i\gamma}(k)|} \tag{46}$$

where the $|\Delta\hat{R}(k)|_{\min}$ denotes the minimum increment of $\hat{R}$ per sampling period, which can be selected by users. $|\cdot|$ is the amplitude value. $e^f_{i\gamma}(k)$ is the injected-frequency component of $e_{i\gamma}(k)$ and can be also estimated by users.

2) Considering the fluctuation from k_{th} to $(k+1)_{th}$ step on the steady state, the maximum fluctuation of $\hat{R}$ can be derived as

$$|\Delta\hat{R}(k)|_{\max} = k_R T(|i_{\gamma\_\mathrm{ref}}| + |i_{\delta\_\mathrm{ref}}|)\xi_{ei} \tag{47}$$

where the ξ_{ei} denotes the boundary of $e_{i\gamma}(k)$ and $e_{i\delta}(k)$ on the steady state. By a predefined maximum fluctuation of $\hat{R}$ and ξ_{ei}, the k_R has to be satisfied as

$$k_R \leq \frac{|\Delta\hat{R}(k)|_{\max}}{T(|i_{\gamma\_\mathrm{ref}}| + |i_{\delta\_\mathrm{ref}}|)\xi_{ei}}. \tag{48}$$

Therefore, the amplitude of the injected signal can be adjusted to make k_R satisfy both (44), (46), and (48). But considering the limited voltage margin of the PWM inverter, there is a tradeoff between the k_R and the amplitude of the injected signal.

2) Selection of k_L: The same procedure mentioned above can be also applied in the selection of k_L. There are

$$k_L \geq 10\xi_L\xi_{\dot{L}} \tag{49}$$

$$k_L \geq \frac{2.83|\Delta\hat{L}(k)|_{\min}}{T|\dot{i}_{\gamma\_\mathrm{ref}}(k)||e^f_{i\gamma}(k)|} \tag{50}$$

$$k_L \leq \frac{|\Delta\hat{L}(k)|_{\max}}{T(|\dot{i}_{\gamma\_\mathrm{ref}}| + \omega|i_{\gamma\_\mathrm{ref}}| + \omega|i_{\delta\_\mathrm{ref}}|)\xi_{ei}} \tag{51}$$

where the $|\Delta\hat{L}(k)|_{\min}$ denotes the minimum increment of $\hat{L}$ per sampling period and the $|\Delta\hat{L}(k)|_{\max}$ is the maximum fluctuation of $\hat{L}$ from k_{th} to $(k+1)_{th}$ step on the steady state. Clearly, because of the existence of the differential term, the amplitude and the frequency of the injected signal can be adjusted to satisfy (49)–(51).

3) Selection of k_e: Based on (34), in order to reduce the tracking error, k_e can be selected as

$$k_e \geq 10\,\omega\xi_{\dot{\psi}_m}(\xi_{e_\gamma} + \xi_{e_\delta}). \tag{52}$$

Besides, when the ω is rapidly increasing or decreasing, the back-EMF also changes with the ω. The estimation of the back-EMF is necessary to have excellent dynamic performance to track this change. Considering the case with the ω ranging from 0 to the rate speed

$$k_e \geq \frac{|\Delta\hat{e}_\delta(k)|_{\min}}{T|e^d_{i\delta}(k)|} \tag{53}$$

where the $|\Delta\hat{e}_\delta(k)|_{\min}$ denotes the minimum increment of $\hat{e}_\delta$ per sampling period. $e^d_{i\delta}(k)$ is the maximum tracking error of the i_δ in the acceleration process. Additionally, considering the fluctuation on the steady state

$$k_e \leq \frac{|\Delta\hat{e}_\delta(k)|_{\max}}{T\xi_{ei}} \tag{54}$$

where $|\Delta\hat{e}_\delta(k)|_{\max}$ denotes the maximum fluctuation of $\hat{e}_\delta$ from k_{th} to $(k+1)_{th}$ step on the steady state. Clearly, the selection of k_e is unrelated with the injected signal.

Finally, based on (34) and the selection method of these gains, the tracking error can be restricted in a small boundary as follows:

$$\sqrt{e^2_{i\gamma} + e^2_{i\delta}} \leq \sqrt{\frac{0.3}{k_{ei} + R}}. \tag{55}$$

C. Operating Mechanism

As the analysis mentioned above, the convergent rate of $\hat{R}$ depends on the selection of k_R and the amplitude of the injected signal. And the convergent rate of $\hat{L}$ depends on not only the

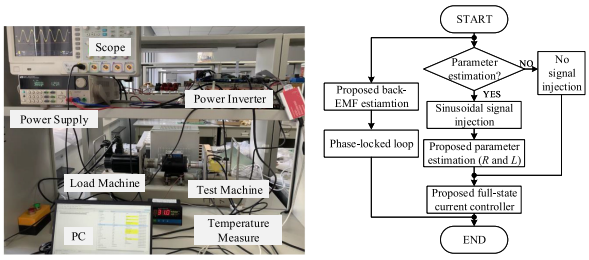

(a) (b)

Fig. 2. Experimental setup and flowchart of the proposed method. (a) Experimental setup. (b) Flowchart.

selection of k_L and the amplitude of the injected signal but also the frequency of the injected signal. Considering L varies much faster than the R and the limited voltage margin, the estimation of R and L is separately executed and the operating mechanism is designed as follows:

1) The estimation of the back-EMF is always executed to achieve the position sensorless drive.
2) The estimation of L is executed before the estimation of R. This injected signal can be selected as a sinusoidal wave with small amplitude and high frequency relatively. Small amplitude is beneficial for the limited voltage margin. High frequency can accelerate the convergence of $\hat{L}$.
3) Then the estimation of R is executed. And this injected signal can be selected as a sinusoidal wave with large amplitude and low frequency relatively. Large amplitude can accelerate the convergence of $\hat{R}$. Low frequency is beneficial for the limited voltage margin.
4) Once any change occurs in the i_δ, the estimation of L is executed immediately.

VI. Validation and Analysis

In this section, first, the gains of the proposed method are calculated and the injected sinusoidal signal is selected. Then simulation is performed in MATLAB/Simulink to verify the proposed adaptive control method and some experiments are also designed. The experimental setup is shown in Fig. 2(a) and the flowchart of the proposed method is demonstrated in Fig. 2(b). Because the speed loop is not of concern in this article, the test SPMSM is driven with torque controlled while the load machine is driven with speed controlled. Besides, an incremental encoder is installed on the shaft of the test SPMSM to obtain the real rotor position.

The parameters of the SPMSM are shown in Table I, which are consistent with the experimental plant. The resistance is measured offline and the inductance with different torque current can be obtained by 3D-finite element method (3D-FEM) tool. The waveforms of the inductance at $i_q = 3$ A and $i_q = 5$ A are shown in Fig. 3(a) and (b), respectively.

The microprocessor adopted in the control board is TMS320F28335 provided by TI and the system clock is 150 MHz. The proposed method is implemented in C code by the Code Composer Studio software. All the data of the experiments

TABLE I
Parameters of the Experimental Plant

Symbol	Parameter	Value
U_{DC}	DC bus voltage	300 V
$poles$	poles of the machine	8
n_N	the rated speed	3000 r/min
i_{qr}	the rated torque current	3A
i_{qm}	the maximum torque current	5A
Po	the rated power	320W
R	resistance (offline)	2.5 Ω
L_s	inductance($i_d = 0$, $i_q = 5$A)(3D-FEM)	5.81 mH
L_s	inductance($i_d = 0$, $i_q = 3$A)(3D-FEM)	6.48 mH
ψ_m	the flux linkage of PM	0.058Wb
f_s	switching frequency	10 kHz
T	sampling period	50 μs

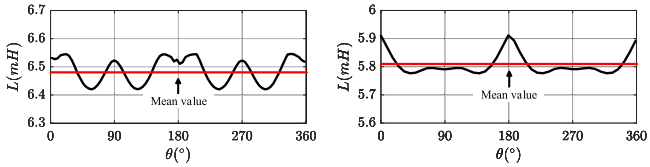

(a) (b)

Fig. 3. Waveforms of the inductance at $i_q = 3$ A and $i_q = 5$ A. (a) Inductance at $i_q = 3$ A. (b) Inductance at $i_q = 5$ A.

TABLE II
Parameters of the Gains Calculation

Symbol	Value	Symbol	Value
ξ_R	10Ω	$\xi_{\dot{R}}$	$5(\Omega/s)$
ξ_L	5mH	$\xi_{\dot{L}}$	$10(mH/s)$
ξ_{e_γ}	1V	ξ_{e_δ}	5V
$\xi_{\dot{\psi}_m}$	$0.1(Wb/s)$	$\lvert e^d_{i\delta}(k)\rvert$	0.1A
$\lvert\Delta\hat{R}(k)\rvert_{min}$	$8T(\Omega)$	$\lvert\Delta\hat{R}(k)\rvert_{max}$	0.05Ω
$\lvert e^f_{i\gamma}(k)\rvert$	0.02 (0.05)	ξ_{ei}	0.1A
$\lvert\Delta\hat{L}(k)\rvert_{min}$	$0.08T(H)$	$\lvert\Delta\hat{L}(k)\rvert_{max}$	$0.5mH$
$\lvert\Delta\hat{e}_\delta(k)\rvert_{min}$	1400T	$\lvert\Delta\hat{e}_\delta(k)\rvert_{max}$	0.2V

are sent to the host PC by the Ethernet module in the control board.

A. Gains Calculation and Signal Selection

The parameters used for the gains calculation are shown in Table II. The maximum torque current is 5 A.

1) For the $|e^f_{i\gamma}(k)|$, when the inductance is being estimated, both the $\hat{R}$ and $\hat{L}$ are inaccurate. But when the resistance is being estimated, the inductance has already converged. Additionally, the inductance value has more effects on the $|e^f_{i\gamma}(k)|$ compared with the resistance. In that case, the $|e^f_{i\gamma}(k)|$ during the inductance estimation is relatively larger than the case during the resistance estimation. So the $|e^f_{i\gamma}(k)|$ is set to be 0.02 and 0.05 A when calculating k_R and k_L, respectively.
2) Selection of $|\Delta\hat{R}(k)|_{\min}$, $|\Delta\hat{L}(k)|_{\min}$, and $|\Delta\hat{e}_\delta(k)|_{\min}$ depends on the desirable convergent rate.

For the selection of k_{ei}, there is

$$-R < k_{ei} \leq \frac{L}{T} - R \tag{56}$$

and

$$-2.5 < k_{ei} \leq 113.5. \tag{57}$$

So the k_{ei} can be selected to be 32 and even with the variable parameters, the tracking error can be still restricted within

$$\sqrt{e_{i\gamma}^2 + e_{i\delta}^2} \leq \sqrt{\frac{0.3}{k_{ei} + R}} = 0.093 \tag{58}$$

1) Resistance Estimation: According to (44), there is

$$k_R \geq 10\xi_R \xi_{\dot{R}} = 500 \tag{59}$$

and based on (46) and (48), it can be derived as

$$k_R \geq \frac{2.83|\Delta\hat{R}(k)|_{\min}}{T|i_{\gamma\_\mathrm{ref}}(k)||e_{i\gamma}^f(k)|} = \frac{1132}{|i_{\gamma\_\mathrm{ref}}(k)|}$$

$$k_R \leq \frac{|\Delta\hat{R}(k)|_{\max}}{T(|i_{\gamma\_\mathrm{ref}}| + |i_{\delta\_\mathrm{ref}}|)\xi_{ei}} = \frac{10000}{|i_{\gamma\_\mathrm{ref}}| + 5}. \tag{60}$$

In order to make these two equations hold, there is

$$|i_{\gamma\_\mathrm{ref}}(k)| \geq 0.64. \tag{61}$$

Therefore, considering the limited voltage margin, the amplitude of the injected signal is selected to be 1 A when the resistance is estimated. Clearly, the frequency of the signal is unrelated to the selection of k_R and it can be selected to be 100 Hz. With the confirmed $|i_{\gamma\_\mathrm{ref}}(k)|$, the k_R has to satisfy as following.

$$1132 \leq k_R \leq 3333. \tag{62}$$

So the k_R is selected to be 1800.

2) Inductance Estimation: According to (49), there is

$$k_L \geq 10\xi_L \xi_{\dot{L}} = 5 \times 10^{-4} \tag{63}$$

and based on (50) and (51), it can be derived as

$$k_L \geq \frac{2.83|\Delta\hat{L}(k)|_{\min}}{T|\dot{i}_{\gamma\_\mathrm{ref}}(k)||e_{i\gamma}^f(k)|} = \frac{4.528}{|\dot{i}_{\gamma\_\mathrm{ref}}(k)|}$$

$$k_L \leq \frac{|\Delta\hat{L}(k)|_{\max}}{T(|\dot{i}_{\gamma\_\mathrm{ref}}| + \omega|i_{\gamma\_\mathrm{ref}}| + \omega|i_{\delta\_\mathrm{ref}}|)\xi_{ei}}$$

$$= \frac{100}{(|\dot{i}_{\gamma\_\mathrm{ref}}| + \omega|i_{\gamma\_\mathrm{ref}}| + 6280)}. \tag{64}$$

To satisfy these two equations, there is

$$A_{inj}(2\pi f_{inj}) - 60A_{inj} - 299 \geq 0 \tag{65}$$

where A_{inj} and f_{inj} is the amplitude and the frequency of the injected signal for the inductance estimation, respectively. With the A_{inj} selected to be 0.5 A, the following equation has to be satisfied.

$$f_{inj} \geq 104.7. \tag{66}$$

So the frequency of injected signal for the inductance estimation is selected to be 400 Hz. For the k_L, there is

$$0.0036 \leq k_L \leq 0.0122 \tag{67}$$

and therefore, the k_L is selected as 0.005.

3) EMF Estimation: According to (52), there is

$$k_e \geq 10\omega\xi_{\dot{\psi}_m}(\xi_{e_\gamma} + \xi_{e_\delta}) = 7536 \tag{68}$$

and based on (46) and (48), it can be derived as

$$k_e \geq \frac{|\Delta\hat{e}_\delta(k)|_{\min}}{T|e_{i\delta}^d(k)|} = 14000$$

$$k_e \leq \frac{|\Delta\hat{e}_\delta(k)|_{\max}}{T\xi_{ei}} = 40000 \tag{69}$$

therefore, k_e is selected to be 25000.

B. Performance on the Steady State

To validate the performance on the steady state, some validations are performed when the tested motor is driven to 3000 r/min. During the process of the acceleration, the parameter estimation for R and L doesn't work and the EMF estimation always works as a model-based observer with the initial parameters ($R = 1\Omega$ and $L = 3$ mH) adopted.

1) Simulation Results: Fig. 4 shows the simulated performance of the proposed method at 3000 r/min. The waveform of the i_γ and i_{γ_ref} are demonstrated in Fig. 4(a)–(c). At 0.1 s, a sinusoidal signal ($0.5\sin(2\pi 400t)$) is injected to estimate the inductance as shown in Fig. 4(b). With the signal injected, the $\hat{L}$ has converged to around 6.42 mH (real inductance: 6.48 mH) within 0.05 s in Fig. 4(d) and this injection will last 0.3 s. At 0.4 s, the other signal ($1\sin(2\pi 100t)$) is injected to estimate the resistance as shown in Fig. 4(c). Fig. 4(e) illustrates the convergent performance of the R and it costs 0.28 s to finish the estimation of the resistance ($\tilde{R} = 0.1\Omega$). After the estimation of R and L, the PM flux linkage can be also calculated correctly in Fig. 4(f). Meanwhile, the performance of the position observation is demonstrated in Fig. 4(g)–(i). The estimated position and the real position before the parameter estimation is shown in Fig. 4(h). Because the mismatched parameters, the estimation error (0.18 rad) occurs inevitably, But after the convergent of the inductance, the estimation error of the rotor position is eliminated as shown in Fig. 4(i). So it can be concluded that the estimation error of the rotor position is unrelated with the resistance in this case.

2) Experimental Results: Fig. 5 shows the experimental performance of the proposed method at 3000 r/min. The same operating process are carried out as the simulation. In Fig. 5(a), the waveform of the the i_γ and i_{γ_ref} are demonstrated. At around 0.12 s, the sinusoidal signal ($0.5\ \sin(2\pi 400t)$) is injected to estimate the inductance as shown in Fig. 5(b). With the signal injected, the $\hat{L}$ has converged to around 6.4mH within 0.05 s in Fig. 5(d) and this injection will last 0.3 s. At around 0.42 s, the other signal ($1\sin(2\pi 100t)$) is injected to estimate the resistance as shown in Fig. 5(c). Fig. 5(e) illustrates the convergent performance of the R and it costs 0.32 s to finish the estimation of the resistance ($\hat{R} = 2.7\Omega$). The estimation of the resistance

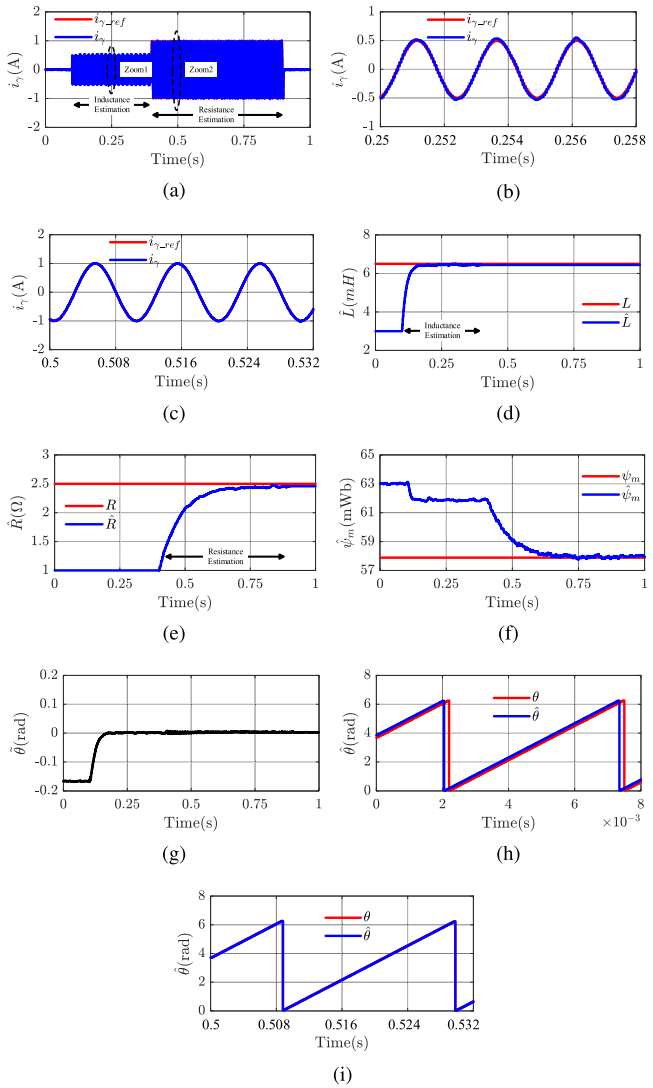

Fig. 4. Simulation results: The performance (i_γ, $\hat{R}$, $\hat{L}$, $\hat{\psi}_m$ and $\tilde{\theta}$) of the proposed method with initial values 1 Ω and 3 mH at 3000 r/min. (a) i_{γ_ref} and i_γ. (b) Zoom1. (c) Zoom2. (d) $\hat{L}$. (e) $\hat{R}$. (f) $\hat{\psi}_m$. (g) $\tilde{\theta}$. (h) $\hat{\theta}$ and θ before estimation. (i) $\hat{\theta}$ and θ after parameter estimation.

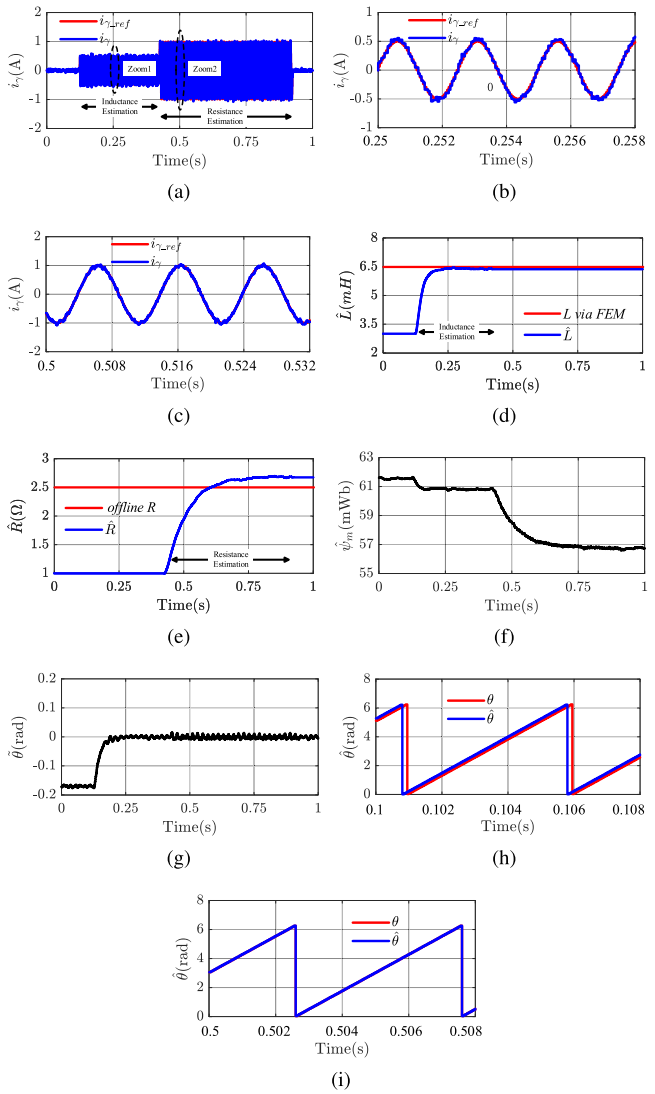

Fig. 5. Experimental results: The performance (i_γ, $\hat{R}$, $\hat{L}$, $\hat{\psi}_m$ and $\tilde{\theta}$) of the proposed method with initial values 1 Ω and 3 mH at 3000 r/min. (a) i_{γ_ref} and i_γ. (b) Zoom1. (c) Zoom2. (d) $\hat{L}$. (e) $\hat{R}$. (f) $\hat{\psi}_m$. (g) $\tilde{\theta}$. (h) $\hat{\theta}$ and θ before estimation. (i) $\hat{\theta}$ and θ after parameter estimation.

may be affected by the wire resistance and the nonlinearity of the PWM inverter, but the estimation error is relatively small to be neglected. After the estimation of R and L, the PM flux linkage can be also calculated correctly in Fig. 5(f). Meanwhile, the performance of the position observation is demonstrated in Fig. 5(g)–(i). The estimated position and the real position before the parameter estimation is shown in Fig. 5(h). Because of the mismatched parameters, the estimation error (0.18 rad) occurs inevitably, but after the convergence of the inductance, the estimation error of the rotor position is eliminated as shown in Fig. 5(i), which indicates the inductance is estimated successfully. And the fluctuation of the position estimation error will be less than 0.02 rad.

Fig. 6 shows the performance of the proposed method at 150 r/min. It can be easily observed that the effectiveness of the proposed method is still guaranteed.

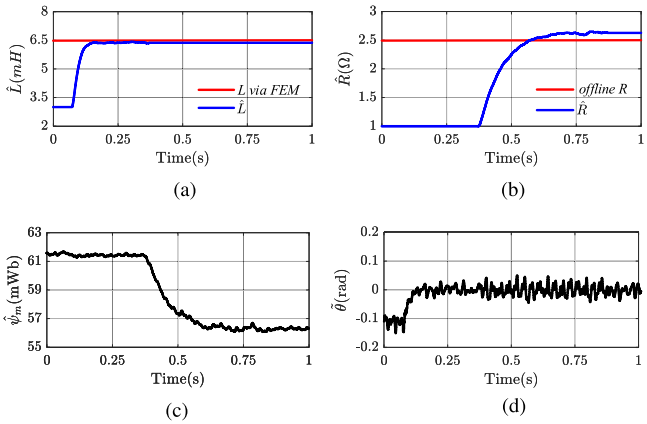

Fig. 6. Experimental results: The performance of the proposed method at 150 r/min. (a) $\hat{L}$. (b) $\hat{R}$. (c) $\hat{\psi}_m$. (d) $\tilde{\theta}$.

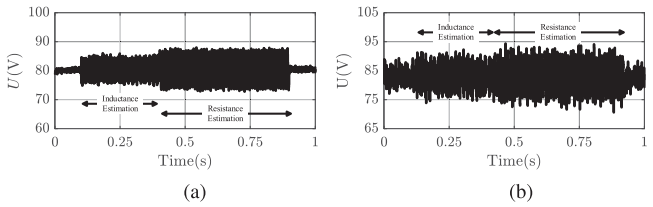

Fig. 7. Simulation and Experimental results: The amplitude of the voltage vector with $i_\delta = 3$ A at 3000 r/min ($U = \sqrt{u_{\gamma c}^2 + u_{\delta c}^2}$). (a) Simulation result. (b) Experiment result.

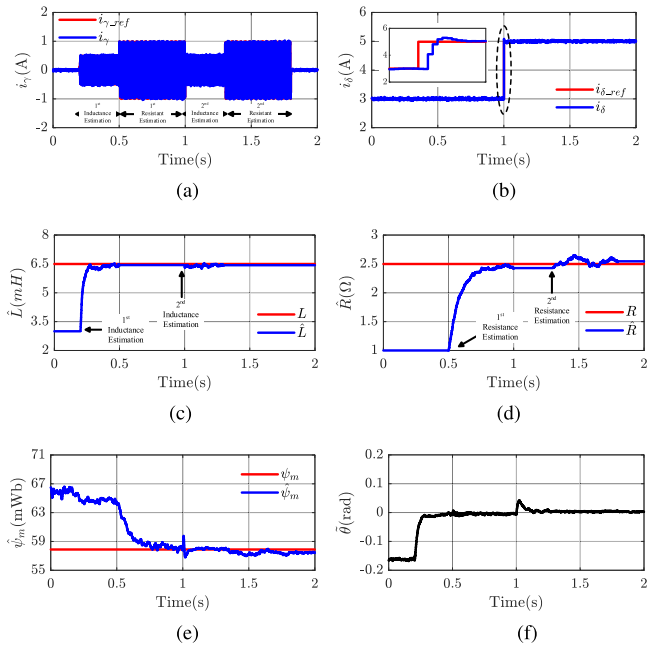

Fig. 8. Simulation results: The performance of the proposed method with step response of i_δ from 3 A to 5 A at 3000 r/min. (a) i_{γ_ref} and i_γ. (b) i_{δ_ref} and i_δ. (c) $\hat{L}$. (d) $\hat{R}$. (e) $\hat{\psi}_m$. (f) $\tilde{\theta}$.

3) Voltage Margin: Because the extra signal needs to be injected, the voltage margin is limited to the implementation. The amplitude of the voltage vector $U = \sqrt{u_{\gamma c}^2 + u_{\delta c}^2}$ is used to evaluate the extra increased voltage caused by the signal injection. The simulated and experimental results are shown in Fig. 7(a) and (b), respectively. These results demonstrate that only around 7 V extra voltage is increased. For the test SPMSM with the rated voltage up to 300 V, it is acceptable by the selection method of the gains and injected signal proposed in this article.

C. Performance on Torque Change

The performance of the proposed method with the torque changing from 3 to 5 A is also validated when the speed still stays 3000 r/min.

1) Simulation Results: Fig. 8 demonstrates the simulated performance of the proposed method with step response of i_δ from 3 to 5 A at 3000 r/min. Before the step response (at 1 s), the performance is same as the case on the steady state. At 1 s, in Fig. 8(b), the i_δ is stepping from 3 to 5 A with

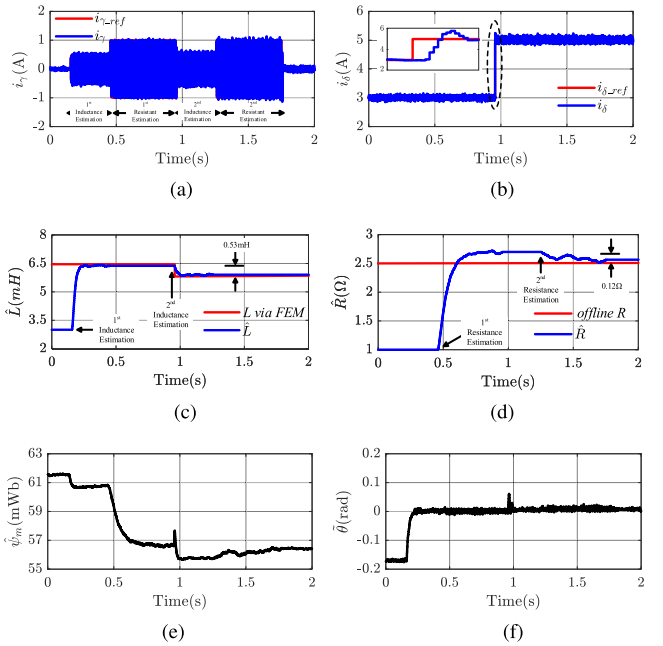

Fig. 9. Experimental results: The performance of the proposed method with step response of i_δ from 3 A to 5 A at 3000 r/min. (a) i_{γ_ref} and i_γ. (b) i_{δ_ref} and i_δ. (c) $\hat{L}$. (d) $\hat{R}$. (e) $\hat{\psi}_m$. (f) $\tilde{\theta}$.

a good dynamic response. Once any change occurs in the i_δ, the estimation of L is executed immediately. So the sinusoidal signal $(0.5\sin(2\pi 400t))$ is immediately injected to estimate the inductance again as shown in Fig. 8(a). The estimated inductance is still around the real value in Fig. 8(c) while the estimation of the R has a little increase by 0.1Ω. As shown in Fig. 8(e), the $\hat{\psi}_m$ almost stays unchanged. For the position observation, the estimation error of the rotor position is shown in Fig. 8(f) and it can be limited within 0.01 rad.

2) Experimental Results: Fig. 9 demonstrates the experimental performance of the proposed method with step response of i_δ from 3 to 5 A at 3000 r/min. At 0.95 s, in Fig. 9(b), the i_δ is stepping from 3 to 5 A. Once any change occurs in the i_δ, the estimation of L is executed immediately. So the sinusoidal signal $(0.5\sin(2\pi 400t))$ is immediately injected to estimate the inductance again as shown in Fig. 9(a). The estimated inductance has a decrease by 0.53mH compared with the estimated inductance values with $i_\delta = 3$ A in Fig. 9(c), which may result from the magnetic saturation. The estimated resistance has a little decrease by 0.12Ω, which is different from the simulated performance. This case explains that, with the increase of the current, the nonlinearity of the PWM inverter has more effects on the resistance estimation, but the small decrease can be neglected compared with the nominal value. The convergence of the estimated flux linkage is demonstrated in Fig. 9(e). For the position observation, the estimation error of the rotor position is shown in Fig. 9(f) and it can be limited within 0.02 rad.

Fig. 10 shows the performance of the proposed method with a step response of the torque when i_δ current changes from 3

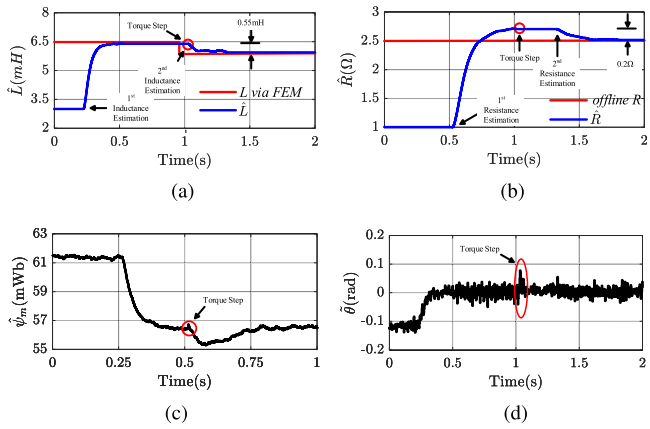

Fig. 10. Experimental results: The performance of the proposed method with step response of i_δ from 3 A to 5 A at 150 r/min. (a) $\hat{L}$. (b) $\hat{R}$. (c) $\hat{\psi}_m$. (d) $\tilde{\theta}$.

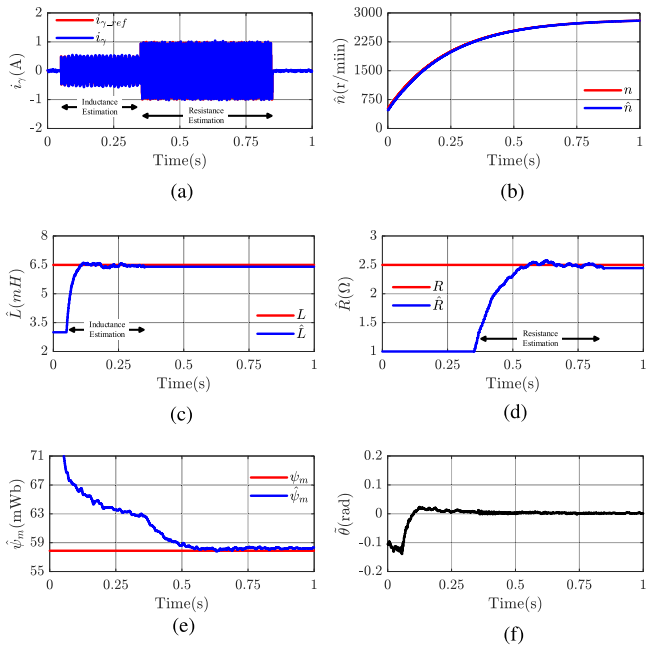

Fig. 11. Simulation results: The performance of the proposed method with the speed accelerating from 1000 to 2500 r/min. (a) i_{γ_ref} and i_γ. (b) $\hat{n}$. (c) $\hat{L}$. (d) $\hat{R}$. (e) $\hat{\psi}_m$. (f) $\tilde{\theta}$.

to 5 A at 150 r/min. It keeps consistent with the performance at 3000 r/min.

D. Performance of Speed Change

The performance of the proposed method with the speed changing from 1000 to 2500 r/min is also validated when the torque current stays 3 A.

1) Simulation Results: Fig. 11 demonstrates the simulated performance of the proposed method with the speed accelerating from 1000 to 2500 r/min. The estimated speed and the real speed are shown in Fig. 11(b). In Fig. 11(c)–(e), the accurate estimation is still established for the inductance, the resistance, and the flux linkage of the PM, respectively. The estimation error of the rotor position is shown in Fig. 11(f). During the accelerating process, after the inductance estimation, the maximum $\tilde{\theta}$ is still less than 0.02 rad.

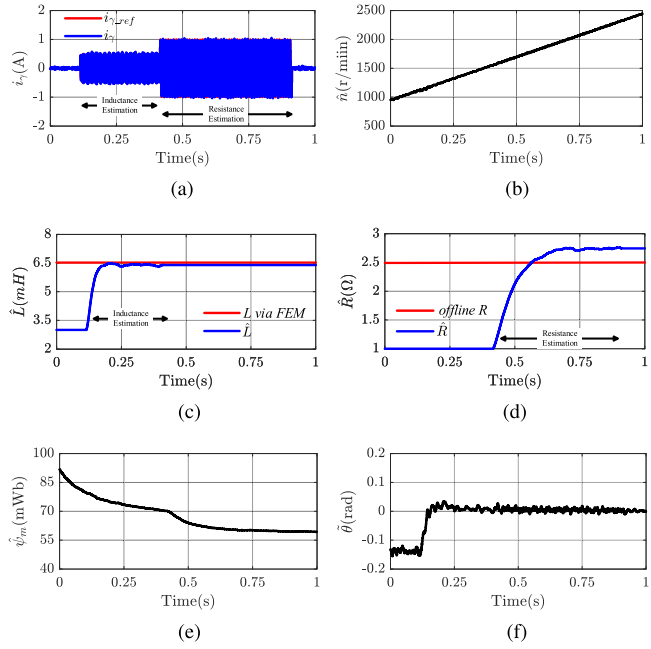

Fig. 12. Experimental results: The performance of the proposed method with the speed accelerating from 1000 to 2500 r/min. (a) i_{γ_ref} and i_γ. (b) $\hat{n}$. (c) $\hat{L}$. (d) $\hat{R}$. (e) $\hat{\psi}_m$. (f) $\tilde{\theta}$.

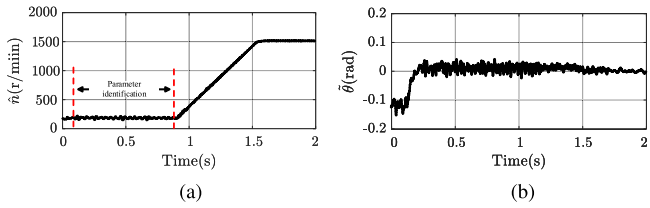

Fig. 13. Experimental results: The transient performance of the proposed method from 150 to 1500 r/min with the estimated parameter at 150 r/min. (a) $\hat{n}$. (b) $\tilde{\theta}$.

2) Experimental Results: Fig. 12 demonstrates the experimental performance of the proposed method with the speed accelerating from 1000 to 2500 r/min. The estimated speed is shown in Fig. 12(b). Fig. 12(c)–(e) illustrate the estimation performance for the inductance, the resistance and the flux linkage of the PM, respectively, which is same as the performance at 3000 r/min. The estimation error of the rotor position is shown in Fig. 12(f). During the accelerating process, after the inductance estimation, the maximum $\tilde{\theta}$ is still less than 0.03 rad.

Fig. 13 shows the transient performance of the proposed method from 150 to 1500 r/min. The adopted parameters are estimated on the steady state at 150 r/min. It can be easily observed that the estimation error of the position keeps small during the acceleration, which indicates the estimated parameters are still accurate.

Fig. 14 shows the performance of the proposed method with the speed loop from 0 to 3000 r/min. The load machine is

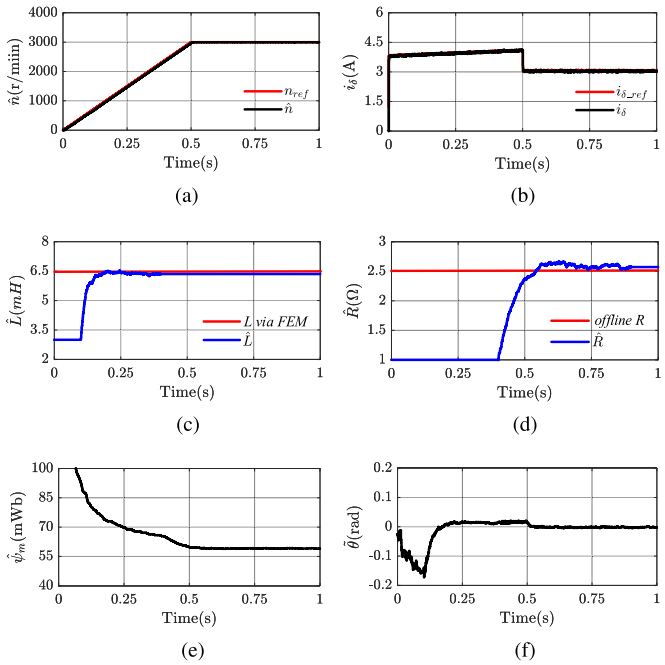

Fig. 14. Experimental results: The performance of the proposed method with the speed loop from 0 to 3000 r/min. (a) n_{ref} and $\hat{n}$. (b) i_{δ_ref} and i_δ. (c) $\hat{L}$. (d) $\hat{R}$. (e) $\hat{\psi}_m$. (f) $\tilde{\theta}$.

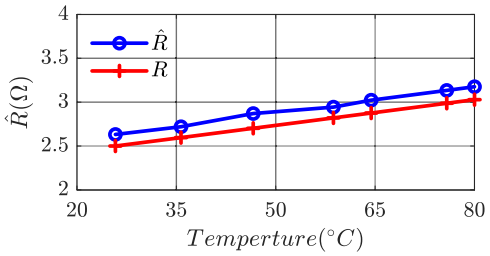

Fig. 15. Experimental results: Resistance estimation with temperature variation from 25 °C to 80 °C.

controlled by the given torque. The reference of the speed is a ramp signal, which can reach to 3000 r/min within 0.5 s as shown in Fig. 14(a). With the proposed adaptive controller, i_{δ_ref} can be well tracked by the i_δ. At the same time, the R, L, and ψ_m are well estimated. Besides, the estimation error of the rotor position can be controlled within 0.02 rad even during the acceleration.

E. Resistance with Temperature Variation

Fig. 15 shows the resistance estimation with temperature variation from 25 °C to 80 °C, of which the blue line represents the estimated resistance and the black line represents the theoretical resistance. The theoretical resistance is calculated based on the temperature as $R_t = R_{25\,^\circ\text{C}}(1 + 0.0039(t - 25\,^\circ C))$. Where, t is the instant temperature and $R_{25\,^\circ\text{C}} = 2.5\,\Omega$. The estimation of the resistance may be affected by the wire resistance and the nonlinearity of the PWM inverter. Besides, the measured temperature is the temperature of the surface of the tested motor, which is a little smaller than the temperature of the stator winding. But the estimation error is still relatively small. Moreover, the gradually increasing trend and the increment with the temperature variation is well tracked by the proposed method.

Based on the analysis of the simulation and experimental results, the effectiveness of the proposed method is guaranteed when the test motor is on the steady state, torque change, and speed change.

F. Comparison of the Execution Time

The execution time of the parameter estimation is compared between the proposed method and the existing method [25]. The execution time is obtained by a timer in parallel. The detail of the algorithm in [25] will not be provided in this article. The result of this comparison is demonstrated as follows.

Method	Execution Time	
	Parameter Estimation	Sensorless Drive
Method in [25]	9.687μs	1.38μs
Proposed Method	0.426 μs	1.07μs

It can be easily observed that the execution time of the proposed parameter estimation and the position sensorless drive have been significantly reduced compared with the method in [25]. The execution time of the whole method is approximately 1.496 μs, which is beneficial for the industrial application.

VII. Conclusion

This article proposes a position sensorless drive and online parameter estimation method for SPMSM based on adaptive full-state feedback current control. The proposed adaptive method has several advantages.

1) The current control with adaptive full-state feedback for position sensorless drive is designed to achieve fast tracking performance with enhanced robustness.
2) Online parameter estimation for R, L, and ψ_m are achieved for a sensorless SPMSM drive system.
3) The performance of position estimation is greatly improved and is totally immune to parameter variations.
4) The stability is well guaranteed by the selected Lyapunov function compared with [25].
5) The execution time of the proposed method is much reduced because the matrix manipulations are avoided compared with the existing methods [22], [25]. Additionally, the proposed method includes the current regulator, sensorless drive, and parameter estimation, which indicates all the crucial control parts for a sensorless PMSM drive system are investigated in this article. Therefore, with the reduced execution time and the comprehensive control, it is easy to be implemented in the industrial applications.

Appendix

For the estimation of R, the phase difference between $i_{\gamma\_\text{ref}}(k)$ and $e_{i\gamma}(k)$ can be selected as follows.

According to the design of the proposed method, the estimation of L is given priority. It indicates that when the R is identified, the $\tilde{L}$ has converged to zero. So the dynamic response of the $e_{i\gamma}$ can be simplified as

$$\dot{e}_{i\gamma} = -\frac{k_{ei}+R}{L}e_{i\gamma} + \frac{\tilde{R}}{L}i_{\gamma\_\mathrm{ref}} + \frac{1}{L}\tilde{e}_{\gamma} \tag{70}$$

based on (6) and (21), it can be obtained as

$$\dot{\tilde{e}}_{\gamma} = -\tilde{e}_{\delta}\dot{\tilde{\theta}} - \omega\dot{\psi}_m \sin\tilde{\theta} - k_e e_{i\gamma}. \tag{71}$$

Considering the $\dot{\tilde{\theta}}$ and $\tilde{\theta}$ vary slowly, it can be simplified as

$$\dot{\tilde{e}}_{\gamma} = -k_e e_{i\gamma}. \tag{72}$$

Therefore, it can be derived as

$$\begin{aligned}\ddot{e}_{i\gamma} &= -\frac{k_{ei}+R}{L}\dot{e}_{i\gamma} + \frac{\tilde{R}}{L}\dot{i}_{\gamma\_\mathrm{ref}} + \frac{1}{L}\dot{\tilde{e}}_{\gamma} \\ &= -\frac{k_{ei}+R}{L}\dot{e}_{i\gamma} + \frac{\tilde{R}}{L}\dot{i}_{\gamma\_\mathrm{ref}} - \frac{1}{L}k_e e_{i\gamma}\end{aligned} \tag{73}$$

and

$$e_{i\gamma}(s) = \frac{\tilde{R}s}{Ls^2 + (k_{ei}+R)s + k_e} i_{\gamma\_\mathrm{ref}}(s). \tag{74}$$

The phase difference between $i_{\gamma\_\mathrm{ref}}(k)$ and $e_{i\gamma}(k)$ can be easily calculated and it is totally unrelated with the $\tilde{R}$. Assuming that L ranges from 5 to 10 mH, R varies from 1 to 5 Ω, $k_{ei} = 32$, and $k_e = 25\,000$, the phase difference is calculated by the MATLAB tool and it ranges from 0.2333 to 0.2658π. For averaging this variation, the phase difference is selected to be 0.25π.

REFERENCES

[1] G. Wang, L. Yang, G. Zhang, X. Zhang, and D. Xu, "Comparative investigation of pseudorandom high-frequency signal injection schemes for sensorless IPMSM drives," *IEEE Trans. Power Electron.*, vol. 32, no. 3, pp. 2123–2132, Mar. 2017.

[2] X. Zhang, H. Li, S. Yang, and M. Ma, "Improved initial rotor position estimation for PMSM drives based on HF pulsating voltage signal injection," *IEEE Trans. Ind. Electron.*, vol. 65, no. 6, pp. 4702–4713, Jun. 2018.

[3] Q. Tang, A. Shen, X. Luo, and J. Xu, "IPMSM sensorless control by injecting Bi-directional rotating HF carrier signals," *IEEE Trans. Power Electron.*, vol. 33, no. 12, pp. 10698–10707, Dec. 2018.

[4] J.-I. Ha, K. Ide, T. Sawa, and S.-K. Sul, "Sensorless rotor position estimation of an interior permanent-magnet motor from initial states," *IEEE Trans. Ind. Appl.*, vol. 39, no. 3, pp. 761–767, May 2003.

[5] S. Chi, Z. Zhang, and L. Xu, "Sliding-mode sensorless control of direct-drive PM synchronous motors for washing machine applications," *IEEE Trans. Ind. Appl.*, vol. 45, no. 2, pp. 582–590, Mar. 2009.

[6] Z. Qiao, T. Shi, Y. Wang, Y. Yan, C. Xia, and X. He, "New sliding-mode observer for position sensorless control of permanent-magnet synchronous motor," *IEEE Trans. Ind. Electron.*, vol. 60, no. 2, pp. 710–719, Feb. 2013.

[7] T. Bernardes, V. F. Montagner, H. A. Gründling, and H. Pinheiro, "Discrete-time sliding mode observer for sensorless vector control of permanent magnet synchronous machine," *IEEE Trans. Ind. Electron.*, vol. 61, no. 4, pp. 1679–1691, Apr. 2014.

[8] J. Choi, K. Nam, A. A. Bobtsov, A. Pyrkin, and R. Ortega, "Robust adaptive sensorless control for permanent-magnet synchronous motors," *IEEE Trans. Power Electron.*, vol. 32, no. 5, pp. 3989–3997, May 2017.

[9] A. Piippo, M. Hinkkanen, and J. Luomi, "Analysis of an adaptive observer for sensorless control of interior permanent magnet synchronous motors," *IEEE Trans. Ind. Electron.*, vol. 55, no. 2, pp. 570–576, Feb. 2008.

[10] S. Po-ngam and S. Sangwongwanich, "Stability and dynamic performance improvement of adaptive full-order observers for sensorless PMSM drive," *IEEE Trans. Power Electron.*, vol. 27, no. 2, pp. 588–600, Feb. 2012.

[11] D. Bao, X. Pan, Y. Wang, X. Wang, and K. Li, "Adaptive synchronous-frequency tracking-mode observer for the sensorless control of a surface PMSM," *IEEE Trans. Ind. Appl.*, vol. 54, no. 6, pp. 6460–6471, Nov. 2018.

[12] T. Michalski, C. Lopez, A. Garcia, and L. Romeral, "Sensorless control of five phase PMSM based on extended Kalman filter," in *Proc. 42nd Annu. Conf. IEEE Ind. Electron. Soc.*, Oct. 2016, pp. 2904–2909.

[13] K. Liu, Q. Zhang, J. Chen, Z. Q. Zhu, and J. Zhang, "Online multiparameter estimation of nonsalient-pole PM synchronous machines with temperature variation tracking," *IEEE Trans. Ind. Electron.*, vol. 58, no. 5, pp. 1776–1788, May 2011.

[14] S. J. Underwood and I. Husain, "Online parameter estimation and adaptive control of permanent-magnet synchronous machines," *IEEE Trans. Ind. Electron.*, vol. 57, no. 7, pp. 2435–2443, Jul. 2010.

[15] T. Boileau, N. Leboeuf, B. Nahid-Mobarakeh, and F. Meibody-Tabar, "Online identification of PMSM parameters: Parameter identifiability and estimator comparative study," *IEEE Trans. Ind. Appl.*, vol. 47, no. 4, pp. 1944–1957, Jul. 2011.

[16] W. Deng, C. Xia, Y. Yan, Q. Geng, and T. Shi, "Online multiparameter identification of surface-mounted PMSM considering inverter disturbance voltage," *IEEE Trans. Energy Convers.*, vol. 32, no. 1, pp. 202–212, Mar. 2017.

[17] D. Q. Dang, M. S. Rafaq, H. H. Choi, and J. Jung, "Online parameter estimation technique for adaptive control applications of interior PM synchronous motor drives," *IEEE Trans. Ind. Electron.*, vol. 63, no. 3, pp. 1438–1449, Mar. 2016.

[18] Z. Liu, H. Wei, Q. Zhong, K. Liu, X. Xiao, and L. Wu, "Parameter estimation for VSI-Fed PMSM based on a dynamic PSO with learning strategies," *IEEE Trans. Power Electron.*, vol. 32, no. 4, pp. 3154–3165, Apr. 2017.

[19] S. Li, J. Fang, and B. Han, "High-precision parameter identification of high-speed magnetic suspension motor," *IEEE Trans. Energy Convers.*, vol. 33, no. 1, pp. 20–31, Mar. 2018.

[20] O. C. Kivanc and S. B. Ozturk, "Sensorless PMSM drive based on stator feedforward voltage estimation improved with MRAS multiparameter estimation," *IEEE/ASME Trans. Mechatronics*, vol. 23, no. 3, pp. 1326–1337, Jun. 2018.

[21] S. Ichikawa, M. Tomita, S. Doki, and S. Okuma, "Sensorless control of permanent-magnet synchronous motors using online parameter identification based on system identification theory," *IEEE Trans. Ind. Electron.*, vol. 53, no. 2, pp. 363–372, Apr. 2006.

[22] M. A. Hamida, J. D. Leon, A. Glumineau, and R. Boisliveau, "An adaptive interconnected observer for sensorless control of PM synchronous motors with online parameter identification," *IEEE Trans. Ind. Electron.*, vol. 60, no. 2, pp. 739–748, Feb. 2013.

[23] A. Piippo, M. Hinkkanen, and J. Luomi, "Adaptation of motor parameters in sensorless PMSM drives," *IEEE Trans. Ind. Appl.*, vol. 45, no. 1, pp. 203–212, Jan. 2009.

[24] D. Liang, J. Li, and R. Qu, "Sensorless control of permanent magnet synchronous machine based on second-order sliding-mode observer with online resistance estimation," *IEEE Trans. Ind. Appl.*, vol. 53, no. 4, pp. 3672–3682, Jul. 2017.

[25] M. S. Rafaq, F. Mwasilu, J. Kim, H. H. Choi, and J. Jung, "Online Parameter identification for model-based sensorless control of interior permanent magnet synchronous machine," *IEEE Trans. Power Electron.*, vol. 32, no. 6, pp. 4631–4643, Jun. 2017.

[26] J.-J. Slotine and W. Li, *Applied Nonlinear Control*. Englewood Cliffs, NJ, USA: Prentice–Hall, Oct. 1990. [Online]. Available: https://book.douban.com/subject/2972704/

[27] F. Peng, J. Ye, A. Emadi, and Y. Huang, "Position sensorless control of switched reluctance motor drives based on numerical method," *IEEE Trans. Ind. Appl.*, vol. 53, no. 3, pp. 2159–2168, May 2017.

Yu Yao (S'18) received the B.S. degree in electrical engineering from Southeast University, Nanjing, China, in 2016. He is currently working toward the doctor of Engineering in electric machines and control at School of Electrical Engineering, Southeast University, Nanjing, China.

His main research interests include the design of the power inverter, the current regulator design, the position sensorless drive for the high-speed PSMSM and the drive system with LCL output filter.

Yunkai Huang received the M.Sc. and Ph.D. degrees in electrical engineering from the Southeast University, Nanjing, China, in 2001 and 2007, respectively.

He is currently a Professor with the School of Electrical Engineering, Southeast University. His research interests include design and control of PM machine and high speed machine, applications in domestic appliances, electric vehicles, railway traction, all-electric ships, more-electric aircraft, and wind power generation systems.

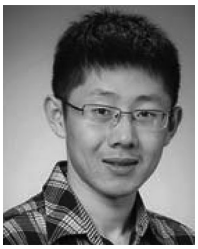

Fei Peng (S'15–M'16) received the B.S. and M.S. in electrical engineering from Southeast University, Nanjing, China, in 2010 and 2012, respectively. He received his Ph.D. degree in electrical and computer Engineering from McMaster University, Hamilton, ON, Canada, in 2016.

He has worked as a Postdoctoral Fellow with the McMaster Institute for Automotive Research and Technology (MacAUTO), McMaster University. From December 2016, he joined the School of Electrical Engineering at Southeast University, Nanjing, Jiangsu, China, as an Assistant Professor. His research interests include optimal design and control of power converters, modeling and digital control of motor drives.

Jianning Dong (S'10–M'17) received the B.S. and Ph.D. degrees in electrical engineering from Southeast University, Nanjing, China, in 2010 and 2015, respectively.

He is an Assistant Professor at the Delft University of Technology, Delft, Netherlands, since 2016. Before joining TU Delft, he was a Postdoctral Researcher with McMaster Automotive Resource Centre (MARC), McMaster University, Hamilton, ON, Canada. His main research interests are design, modeling and control of electromechanical systems.